Journal of Solid State Chemistry **168,** 343–353 (2002)
doi:10.1006/jssc.2002.9680

Thermal Stability of Pt/Al_2O_3 Catalysts Prepared by Sol–Gel

E. Romero-Pascual,*[,1] A. Larrea,† A. Monzón,* and R. D. González‡

*Depto. Ing. Química y TMA, Facultad de Ciencias, Univ. de Zaragoza, Zaragoza 50009, Spain; †Inst. Ciencia de Materiales de Aragón-CSIC, CPS, Univ. de Zaragoza, Zaragoza 50015, Spain; and ‡Department of Chemical Engineering, Tulane University, New Orleans, Louisiana 70118

Received February 19, 2002; accepted June 13, 2002

A series of Pt/Al_2O_3 catalysts were prepared using a sol–gel method. The influence of several parameters used in the synthesis including: metal content, identity of the metal precursor, and the water/alkoxide ratio on the structural properties of the fresh (dried) and calcined samples were studied. It was found that the BET surface area decreased with an increase in the platinum content. A surface area of 500 m^2/g was obtained following calcination at 773 K. The structure of fresh samples as determined by FTIR corresponded to that of a pseudoboehmite structure. Samples prepared using a water/alkoxide ratio (H_2O/ATB) of 9 showed a well-defined, uniform pore size distribution following calcination at 773 K. Metal dispersions comparable to those obtained using impregnation methods were obtained. Aging studies (calcination at 873 K for 24 h) performed on these catalysts, exhibited sintering behavior which were similar to Pt/Al_2O_3 catalysts prepared by other methods. The sample prepared using a H_2O/ATB ratio of 9 had the highest surface area and was more thermally resistant towards metal sintering. A bimodal metal particle size distribution was observed: some particles exhibited sintering while others of similar size showed a greater thermal stability to sintering. The sample having the largest surface area and the highest thermal stability following thermal treatment was a consequence of a more condensed structure and a higher pore roughness obtained after drying the gel. This enabled the formation of an alumina structure which was more amorphous and limited aggregation of platinum particles due to surface diffusion within the pore structure.

Key Words: **Pt/Al_2O_3; sol–gel; aging; sintering.**

INTRODUCTION

Increasing restrictions in the area of environmental pollution control (1) requires the preparation of catalysts with a higher resistance to temperature fluctuations and changes in the composition of automotive exhaust gases. Due to these new requirements, the thermal stability of supports and the resistance of the metallic phase to sintering are of considerable importance in the design of supported metal catalysts which are subjected to these fluctuations. Currently, three-way catalysts (TWCs) are prepared by supporting noble metals such as Pt, Rh, and (mainly) Pd over an alumina washcoat anchored to a monolithic ceramic substrate (2, 3). Zirconia-doped cerium oxide is usually added to these materials in order to improve oxygen-storage capabilities (4–6). In addition, alumina-supported catalysts are widely used in the petroleum industry in reforming and hydrotreating processes (7).

Regarding the catalyst preparation, the synthesis of supported metal catalysts by the sol–gel method has been developed in recent years (8) as an alternative to the traditional methods (impregnation, coprecipitation). Advantages of the sol–gel technique (8, 9) include the preparation of materials with a greater degree of homogeneity, a better-defined pore size distribution, a higher BET surface areas, and a better control over the microstructural properties of the metallic particles. The purity of the alumina support is also important, because several compounds in small quantities may modify the catalytic behavior. The use of alumina precursors with a high degree of purity can go a long way in eliminating most of these impurities (10). The water/alkoxide ratio, the synthesis temperature, the nature of the alkoxide, and the metal precursor are parameters which influence the final properties of catalysts preparated by the sol–gel method. In fact, the thermal properties of the final alumina are largely controlled by the structure of the hydrolized gel.

Alumina-supported catalysts have been prepared using a sol–gel method (11). The BET surface area of both the calcined (773 K) blank alumina and Pt/Al_2O_3 were high (close to 500 m^2/g). However, aging studies have not previously been performed on these materials. Several thermal deactivation studies related to Pt/Al_2O_3 are reported in the literature. Johnson and Keith (12) reported that platinum redispersion occurred on a commercial

[1] To whom correspondence should be addressed. E-mail: eromero@posta.unizar.es.

0022-4596/02 $35.00

Pt/Al_2O_3 catalyst when heated in dry air between 783 and 850 K. However, temperatures in excess of 850 K result in the sintering of the metal crystallites. Many other studies are in agreement with the rapid sintering of platinum in an oxygen atmosphere (13–16) above 873 K. At these conditions, PtO is unstable and decomposes to O_2 and Pt. In this study, we have prepared different samples of Pt/Al_2O_3 by the sol–gel method while varying synthesis conditions. We have also conducted a study about their thermal stability, of both the support and the metal phase as a function of calcination temperature.

EXPERIMENTAL

Samples were prepared following the method described by Balakrishnan and Gonzalez (11). In order to obtain 10 g of sample, a solution containing aluminum *tri-sec*-butoxide (ATB) in 40 mL of *sec*-butanol was prepared. A platinum salt (H_2PtCl_6 or $Pt(Acac)_2$), dissolved in 10 mL of warm acetone, was added. The resulting solution was thoroughly mixed in a rotavapor. The hydrolysis was performed by adding 40 mL of a water–methanol solution. The resultant mixture was stirred at room temperature for 10 min. It was then heated to 318 K and maintained at that temperature under continual stirring for about 10 min. The sample was then cooled to 307 K and stirred for 1 h or more. Solvent removal was performed in the rotavapor system, with one end open to air in order to evacuate the vapor. To this purpose, the sample was maintained at 333 K for 20 h with continual stirring. The temperature was then raised to 353 K and maintained at that temperature for 1 h. Finally, the remaining solvent was evaporated at 373 K for 30 min. The sample was then dried in an oven at 393 K for a period of 24 h. Following drying, the samples were pretreated in a flow system using the following sequence of steps. First, they were heated under He flow to 773 K at a rate of 10 K/min. At this point, the He flow was switched to an air flow for a period of 2 h.

Two different H_2O/ATB ratios were studied (Table 1) as follows: (i) three (corresponding to a stoichiometric ratio) and (ii) nine. The samples were also prepared using two different precursors: H_2PtCl_6 and $Pt(Acac)_2$. The platinum content was designed to obtain samples having a nominal weight loading of 0.4, 1.5, and 3 wt%. Pt compositions were also determined by ICP (Galbraith Laboratories, Knoxville, TN, USA). Differential thermogravimetry (DTG) and thermogravimetric analysis (TGA) experiments were carried out in a thermogravimetric system (C. I. Electronics, model MK2), by heating the dried (uncalcined) sample to 873 K at a heating rate of 10 K/min, under a flow of O_2 (3%) using nitrogen as the carrier gas. The BET surface area and pore size distribution were measured by calculating the N_2 adsorption–desorption isotherm in a Coulter Omnisorb 100 CX apparatus. XRD spectra of the calcined samples were obtained in a Rigaku/Max diffractometer equipped with a rotatory Cu anode. The mean Pt crystallite size was calculated from these spectra by XRD-LB (X-ray Diffraction Line-Broadening) (Scherrer equation) from the (311) reflection of platinum. A pulse technique was used to conduct the H_2 chemisorption in order to obtain the metallic dispersion. Typically, 0.2 g of pretreated sample (calcined at 773 or 873 K) was placed in a quartz microreactor. The sample was heated to 773 K in Ar. It was then reduced in situ in a hydrogen flow at this temperature for 2 h. Adsorbed hydrogen was removed by flowing Ar over the catalyst at 793 K for 1 h. After cooling to room temperature, the chemisorption was carried out introducing hydrogen pulses into the Ar carrier gas. The H_2 pulses were detected using the thermal conductivity detector of an HP 5890 gas chromatograph. In order to check the correspondence between crystallite sizes and metallic dispersion, the particle diameters were obtained using the method described by Spenadel and Boudart (17):

$$d_{Pt} = \frac{846}{D} \qquad [1]$$

where d_{Pt} is the Pt particle diameter (Å) and D is the metallic dispersion (%).

The samples were also examined by transmission electron microscopy (TEM) in a JEOL 2000 FXII operated at 200 keV. A few miligrams of each one were dissolved in ethanol and the liquid was sonicated for 15 min. A drop of the solution was placed on a copper grid and dried prior to placing it in the TEM. The diameter of a large number of particles was measured in order to calculate the mean crystallite size of the samples from the TEM micrographs.

A Bruker IFS-55 spectrophotometer was used in order to obtain the infrared spectra of the samples using DRIFT. Analysis of the samples dried at 393 K and calcined at 773 K was performed.

The aging treatment was carried out by heating the dried samples to 873 K at 10 K/min under He flow. Then He flow was then switched to air and the samples were calcined at 873 K for periods of up to 72 h.

TABLE 1
Samples, Synthesis Parameters, and Pt Content Following Calcination at 773 K (2 h)

Sample	Precursor	H_2O/TAB	Pt (%) (teor)	Pt (%) (ICP)
Pt1	$Pt(AcAc)_2$	3	0.4	0.43
Pt2	H_2PtCl_6	3	1.5	1.39
Pt3	H_2PtCl_6	9	1.5	1.44
Pt4	H_2PtCl_6	3	3	2.99

RESULTS AND DISCUSSION

In Table 1, the weight loadings as measured by ICP are tabulated together with the H_2O/TAB ratios used in the synthesis. There is good agreement between the designed Pt content and the measured value obtained by ICP. Structural characterization of dried (uncalcined) samples was carried out by infrared and thermogravimetric analysis. DRIFT spectra are shown in Fig. 1. The bands are typical of those which correspond to pseudoboehmite (18) (also referred to as "gelatinous boehmite"), a poorly crystallized modification of aluminum oxyhydroxide boehmite. The broadband centered at $3400\,cm^{-1}$, contains a small shoulder at approx. $3250\,cm^{-1}$. It is assigned to the stretching vibrations of the O–H bonds adjoining the Al atoms (hydroxyl groups) and the O–H bonds of water contained in the samples. The wideness of the band is characteristic of the different degrees of interactions of the OH bonds. There is a band at $1080\,cm^{-1}$ which is assigned to the bending vibration of these hydroxyl groups. This is somewhat different to the analogous band in boehmite which is centered as a shoulder at $1160\,cm^{-1}$. There are some additional differences to boehmite, where the band structure is better defined: the stretching hydroxyl bands in boehmite are centered at 3297 and $3090\,cm^{-1}$. Several bands are observed in the $1300–1700\,cm^{-1}$ spectral region, corresponding to the bending vibrations of weakly bound molecular water (18), present in the interlamellar spaces of the pseudoboehmite. The intensity of the latter bands is directly proportional to the amount of excess water, in excess of the stoichiometric composition of the oxyhydroxide. It is well known that pseudoboehmite contains more water than boehmite (19). However, this is dependent on the sample synthesis, conditions, and history. The area below $900\,cm^{-1}$ corresponds to the infrared stretching vibrations of Al–O, with characteristic bands at 530, 630, and $880\,cm^{-1}$ for pseudoboehmite (20, 21). Traces of organic solvents used in the preparation of the samples were detected, with bands in the range between 2800 and $3000\,cm^{-1}$ (stretching vibrations of the C–H bonds). This means that the solvents have not been completely removed following drying at 393 K for 24 h.

It is known that crystalline boehmite transforms (in air or under low water vapor pressure) to γ-alumina at about 723 K (19, 22). Poorly crystallized boehmite can be dehydrated at lower temperatures. Several authors report that γ-alumina is formed under low water vapor pressure at temperatures as low as 623 K (22, 23). On the other hand, pseudoboehmite is completely transformed to boehmite at 513 K and 10 Torr water vapor pressure (23). Moreover, pseudoboehmite can be transformed to γ-alumina at temperatures below 623 K (24). Following heating in air at 573 K, pseudoboehmite dehydrates to a poorly crystallized γ-alumina (19).

TGA showed an initial peak due to the loss of adsorbed water (moisture) between 323 and 373 K. At higher temperatures, a progressive loss in weight occurred with sample heating (Fig. 2), with a maximum at approximately 663 K, due to water removal during the phase transformation to γ-alumina. This water loss is somewhat better resolved in the Pt3 sample. Sample Pt4 shows a maximum in weight loss at 593 K, after which a lower rate of decrease is present. A small peak at 798 K is detected in Pt2 and Pt3, and is also attributed to the loss of water during the formation of γ-alumina (25). The total weight loss, exclusive of the weight loss due to the initial dehydration

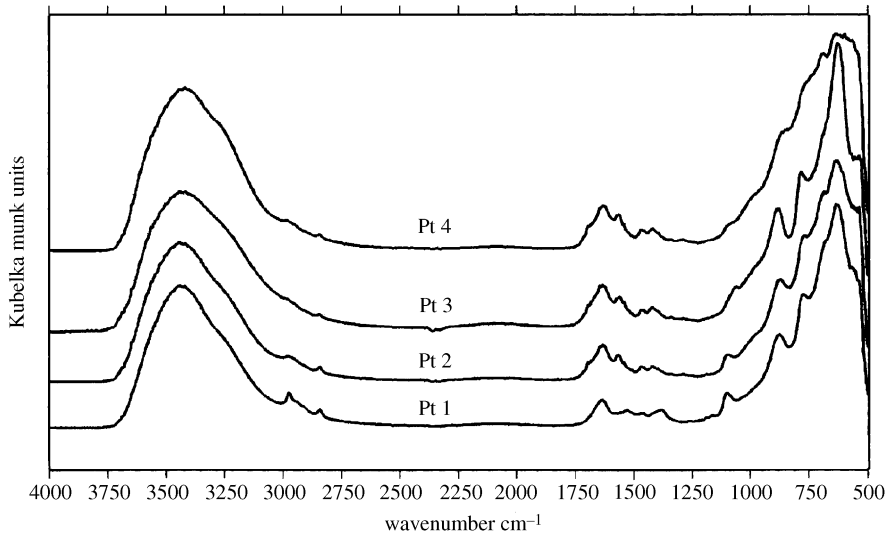

FIG. 1. FTIR spectra of dried samples.

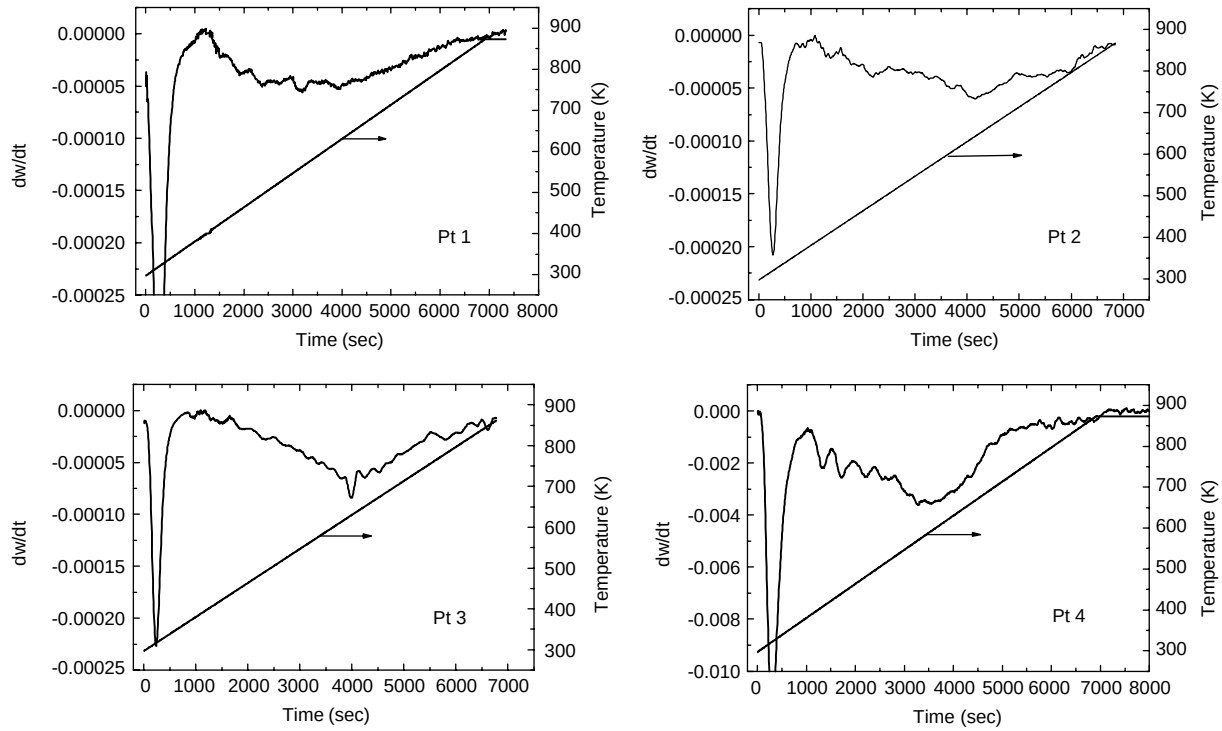

FIG. 2. TGA for the dried samples.

below 473 K, was similar: 21.7%, 19.6%, 18.9%, and 21.6%, respectively, for Pt1, Pt2, Pt3, and Pt4. Sample Pt3 showed a shift to longer times for the starting of removal of OH from the pseudoboehmite structure (above 473 K) than the other samples.

Calcination at 773 K

The characterization results of the samples following calcination at 773 K for 2 h are shown in Table 2. BET surface areas (450–550 m^2/g), are larger than those obtained in traditional γ-aluminas (150–300 m^2/g). This appears to be due to the structural nature of the precursor formed during the preparation of the samples. It has previously been reported (19) that pseudoboehmite has surface areas which are greater than those of the well-crystallized hydroxides or oxyhydroxides. Also an alk-oxide-derived alumina calcined at 773 K (temperature at which the material still remained amorphous) had a surface area as high as 600 m^2/g (26).

TABLE 2
Characteristics of Samples Calcined at 773 K for 2 h

Sample	Pt (wt%)	BET area (m^2/g)	d_p Pt (nm) (TEM)	d_{pore} (nm)	Dispersion Pt (%)	d_p Pt (nm) (from Eq. [1])
Pt1	0.43	550	2.5	4.5, 6.3	32	2.6
Pt2	1.39	537	1.7	4.5, 7	48	1.8
Pt3	1.44	516	1.9	8.2	43	2.0
Pt4	2.99	457	1.5	5.4, 9	56	1.5

The BET surface area decreases with an increase in the Pt content of the catalyst. This suggests that Pt may have an effect on some of the structural parameters of the alumina. These effects may be related to (a) the effect of the platinum precursor on the formation of the pseudoboehmite gel; (b) the effect of the platinum salt during calcination (decomposition of the precursor); (c) both of these. If high BET surface areas are a major consideration, it appears reasonable to keep Pt metal loadings below 1.5%.

Pore size distributions tend toward a bimodal distribution (Fig. 3) with average maxima at 4.5 and 9 nm. However, sample Pt3 was somewhat different. This catalyst had a narrow pore size distribution, with a single maximum at 8.2 nm. An increase in pore size was observed with a decrease in the BET surface area as expected.

The XRD spectra of the samples calcined at 773 K showed amorphous or microcrystalline alumina materials, with no detectable peaks attributed to Pt. Because of X-ray line broadening, this result is of course expected for particles which are smaller than 3–5 nm. The data shown in Table 2 were obtained from TEM observations (Fig. 4). The diameter of the particles was in good agreement with typical values reported in literature, following similar

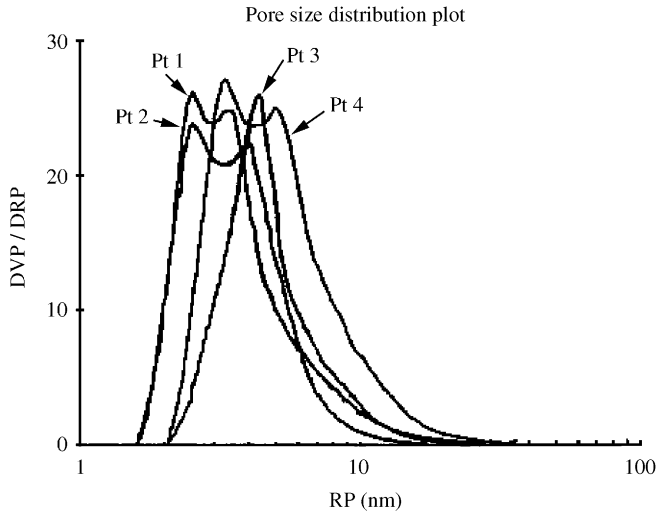

FIG. 3. Pore size (nm) distributions for the samples after calcination at 773 K for 2 h.

treatment conditions. The Pt particles do not have a broad size distribution nor do they have well-faceted shapes, due to the small size of the crystallites. The largest particle diameter was observed for Pt1, which was prepared using $Pt(Acac)_2$ as the metal precursor. This may have been due to the rather poor solubility of the precursor in the solvents used for the synthesis. In fact, the poor solubility was noted during the synthesis, which tended to downplay other possible variables such as salt effects during drying or calcination on the final properties of the material. Indeed Reyes *et al.* (27) and Baltes *et al.* (28) reported a reasonably high dispersion using acetylacetonate as a precursor in comparison to other precursors when the catalysts were prepared by traditional methods. When H_2PtCl_6 was used as the metal precursor in this work, Pt particle sizes were quite similar to results obtained using H_2PtCl_6 by impregnation methods.

In spite of showing the larger BET area, sample Pt1 (prepared using $Pt(Acac)_2$ as the precursor) showed the lowest metallic dispersion (Table 2) in accordance with the higher Pt particle size. As stated earlier, the poor solubility of $P(Acac)_2$ in the solvents appears to be the reason for the low dispersion. Therefore, we observed that, under the synthesis conditions used in this work, the catalysts prepared with chloroplatinic acid as precursor showed better properties than those obtained using $Pt(AcAc)_2$, although the latter sample showed the highest BET surface area.

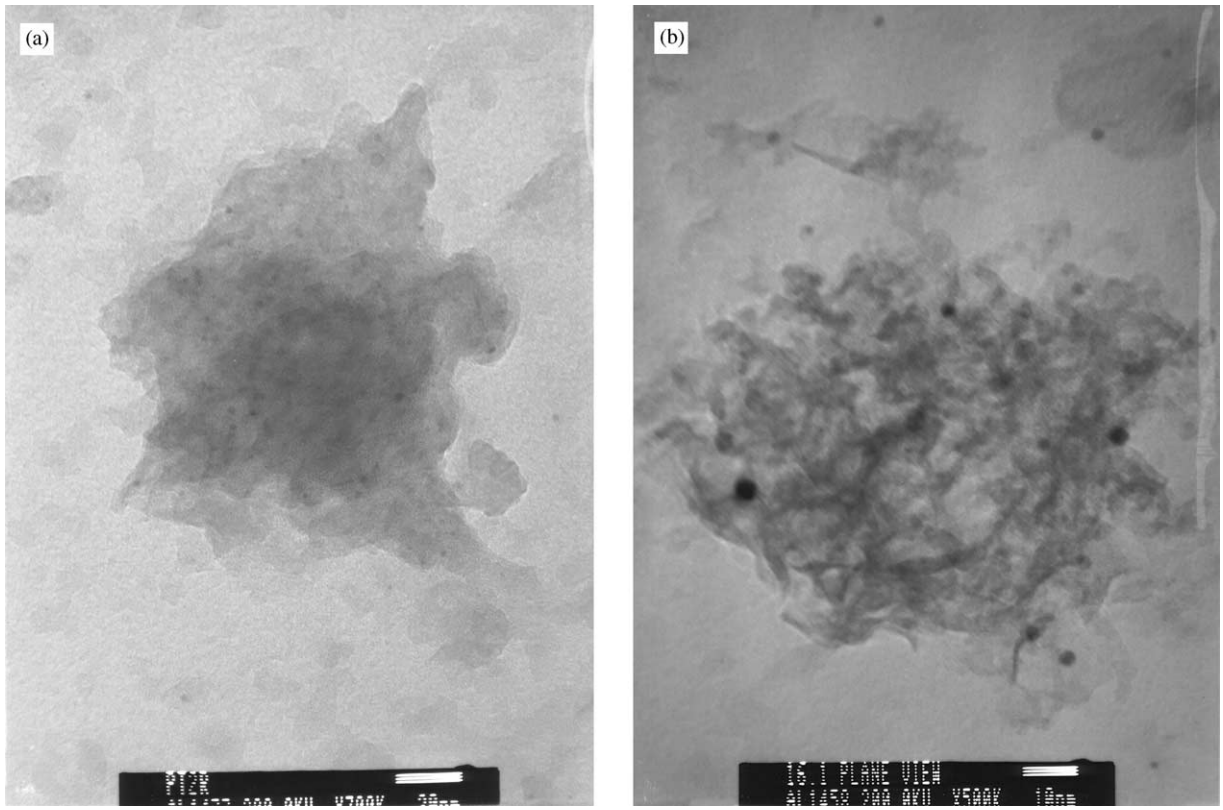

FIG. 4. TEM micrographs of samples Pt2 (a), Pt3 (b), and Pt4 (c) following calcination at 773 K for 2 h. The scales are 20 nm (a), 10 nm (b), and 20 nm (c).

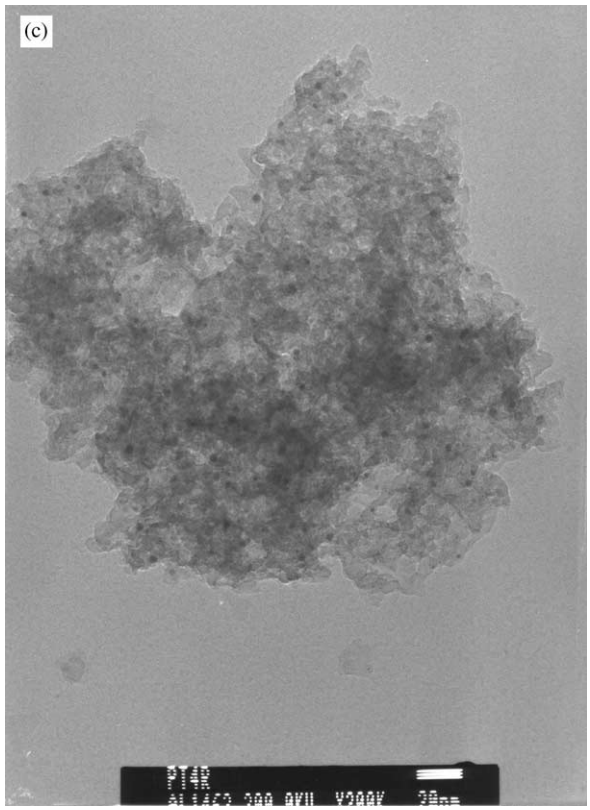

FIG. 4—*Continued*

As the metal particle sizes of the other samples were lower, metallic dispersion values were higher than that in Pt1. Catalyst Pt2 and Pt3 showed similar behavior, although Pt2 had a slightly higher dispersion. Sample Pt4 had the highest dispersion in spite of the increase in Pt metal loading (2.99 wt%, more than twice that of Pt2 and Pt3). Moreover, Pt4 sample had the lowest BET surface area.

The FTIR spectra of samples prepared using H_2PtCl_6 are shown in Fig. 5. The changes in the infrared spectra following calcination at 773 K compared to the those dried at 393 K, were more evident below 1100 cm^{-1}. The characteristic bands of Al–O in γ-alumina can be observed in the 662–580 cm^{-1} spectral region and also at 825 and 745 cm^{-1} (29, 30). These bands are related to the Al atoms present in both octahedral (also present in pseudoboehmite) and tetrahedral sites which are present in the lattice structure. Moreover, the characteristic band of pseudoboehmite at 1080 cm^{-1} is not detected. The wide band due to O–H bonds at approx. 3400 cm^{-1} (with a shoulder at 3250 cm^{-1}) is also present. However, its relative intensity as compared to the Al–O bands below 900 cm^{-1} were less intense than the corresponding bands observed for the samples dried at 393 K. This observation is due to the loss of both OH groups and water. The dehydration of boehmite, pseudoboehmite, and other aluminum hydroxides or oxyhydroxides all undergo water loss from both the hydroxyl groups and the molecular water during heat treatment. However, the transformation from boehmite to γ-alumina occurs as a result of the dehydroxylation. The bands in the 1250–1750 cm^{-1} spectral region, assigned to bending vibrations of OH groups present in interlamellar molecular water, also appeared with less relative intensity following calcination at 773 K.

The average Pt particle size calculated from dispersion measurements has also been included in Table 2. They are

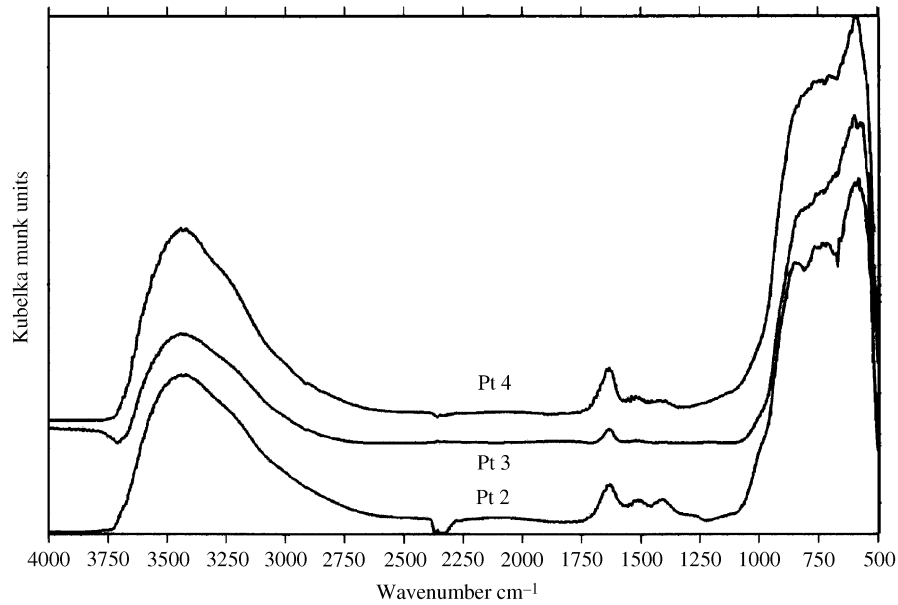

FIG. 5. FTIR spectra of samples prepared using chloroplatinic acid following calcination at 773 K for 2 h.

TABLE 3
Characteristics of Samples Following Calcination at 873 K for 24 h

Sample	BET area (m^2/g)	d_p Pt (nm) (XRD)	d_{pore} (nm)	d_p Pt (nm) (TEM)	Dispersion Pt (%)
Pt1	448	15.0	4.8, 7	—	—
Pt2	384	25.0	5, 8.3	22.2	17
Pt3	435	13.0	9.3	10.0	24
Pt4	324	19.9	4.6, 9.6	18.6	—

in agreement (within experimental error) to those obtained by TEM. As shown here, the sol–gel method results in materials with high dispersions. This result is mainly due to the high BET surface areas obtained in the preparation.

Aging: Calcination at 873 K

Aging experiments, following calcination at 873 K for 24 h, resulted in a general decrease in BET surface area (Table 3): 18.5% in sample Pt1, 28.5% in Pt2, 15.7% in sample Pt3, and 29.1% in Pt4. This decrease was lower for sample Pt3, compared to Pt2 (both Pt2 and Pt3 were prepared using the same Pt loading and Pt precursor). It is of interest to note that samples Pt2 and Pt4, whose only difference was one of metal loading, had a similar loss in surface area (29%). Sample Pt1 also exhibited a loss in surface area which was only slightly higher than that of Pt3.

In parallel with the loss in surface area, pore size distributions were also observed to increase following calcination at 873 K (Fig. 6). Sample Pt3 differed again from the other samples as it was the only material to exhibit a unimodal pore size distribution.

The TEM analysis was used to observe the metal sintering following calcination at 873 K (Fig. 7). The particles appeared mostly well faceted, corresponding to their increase in size. Particle sizes for the larger sintered particles were also calculated by XRD (included in Table 3). Pt3 showed the lowest increase in particle size, resulting in a value of 100 Å. Sample Pt4, which had retained a high dispersion following heating at 773 K (in spite of its high platinum content), was observed to undergo considerable sintering at 873 K. These results can be compared to others reported in the literature for catalysts prepared by impregnation methods. Spenadel and Boudart (17) reported sintering results on a 0.60 wt% Pt supported on η-alumina. The Pt crystallite size was less than 1 nm. Following heating in a hydrogen atmosphere at 923 K for a period of 2 h, the crystallite size increased to 6.1 nm. A 4.46 wt% Pt sample calcined for 24 h at 923 K resulted in an average particle size of 21.2 nm. Further heating for 24 h at 1023 K of a 3.1 wt% Pt catalyst resulted in a particle size of 25.3 nm. Wilson and Hall (31) showed that a 0.75 wt% Pt/Al_2O_3 catalyst exposed to a nitrogen atmosphere at 873 K for 24 h did not sinter. However, 2 h at 895 K in flowing air induced sintering, resulting in an average particle size of 5.3 nm. Ruckenstein and Malhotra (14) prepared a model Pt/alumina catalyst and reported sintering of platinum particles, which grew from a mean size of 3.9 nm (heated at 773 K for 24 h) to 10.7 nm following calcination in air at 873 K for 24 h. The alumina

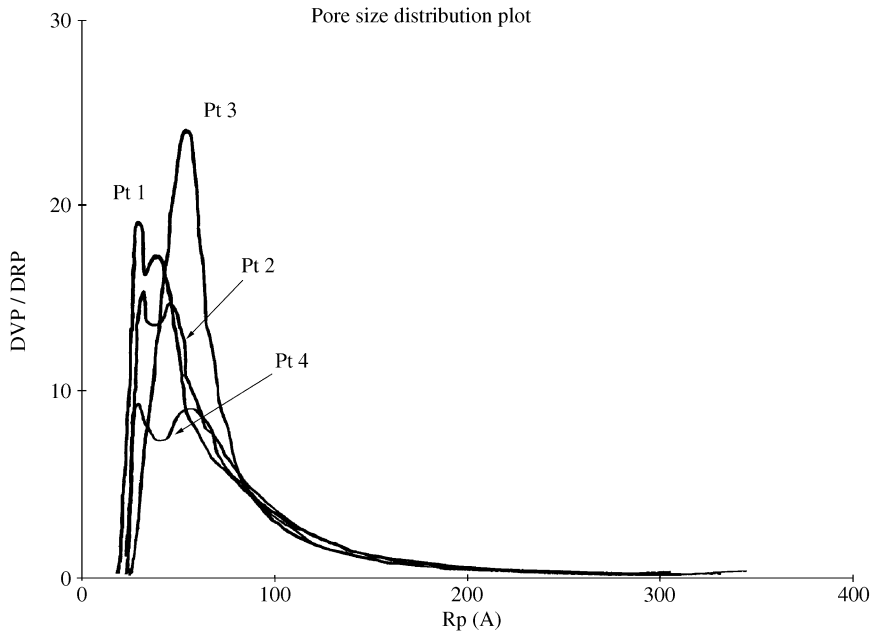

FIG. 6. Pore size (nm) distributions for samples following calcination at 873 K for 24 h.

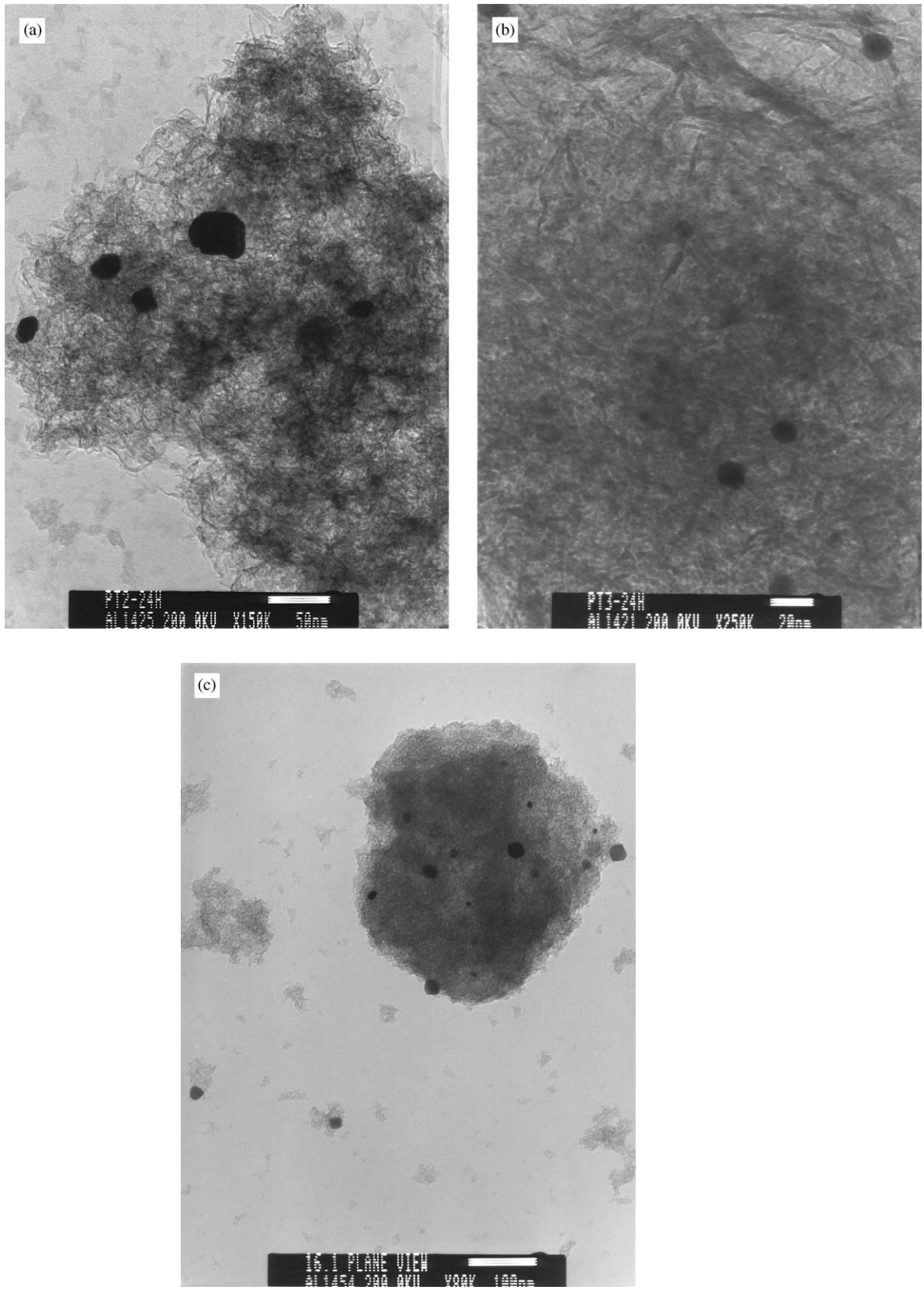

FIG. 7. TEM micrographs of samples Pt2 (a), Pt3 (b), and Pt4 (c) following calcination at 873 K for 24 h. The scales are 50 nm (a), 20 nm (b), and 100 nm (c).

support was previously stabilized by calcination at 873 K for 24 h prior to adding Pt by a sputtering technique. Therefore, sintering results obtained in this study are comparable to others shown in the literature.

Hydrogen chemisorption studies on Pt2 and Pt3 resulted in a high metal dispersion. These values appear to be rather high taking into account particle sizes obtained by XRD. One would expect values in the lower 3–7% range. However, a detailed TEM analysis showed the presence of small metal crystallites (similar in size to those observed following calcination at 773 K), together with the larger sintered particles. The relatively high dispersions are presumably due to the large number of small particles. The particle size distributions corresponding to samples Pt2, Pt3, and Pt4 are shown in Fig. 8. A bimodal pattern was observed for samples Pt2 and Pt3. However, Pt3 had a sharper and narrower particle size distribution. Bimodal distributions have previously been reported (13, 32), and the presence of small crystallites can be related to unsintered particles and/or splitting of the larger particles through oxide formation.

Because Pt3 appeared to be more resistant to sintering, it was subjected to heating at 873 K for a period of 72 h. This treatment resulted in a slight loss in surface area ($390\,m^2/g$) and a small increase in particle size to 10.5 nm. This means that both the loss in BET surface area and the extent of sintering appear to be more dependent on temperature than on heating time. A small increase in the average pore size was also observed following the heat treatment.

From the results shown above, it is clear that sample Pt3 exhibits a higher thermal stability towards sintering than do the other samples. For this reason, it is important to establish how differences in preparative conditions might affect the physical and thermal properties of the different catalysts. Therefore, a comparison between samples with similar Pt content and precursor becomes important. In order to distinguish structural differences between samples Pt2 (water/alkoxide ratio of 3) and Pt3 (water/alkoxide ratio of 9), the thermogravimetric and infrared studies were looked at closely following the drying step.

The differential weight loss analysis showed a slight difference (Fig. 2): following the initial removal of water (below 473 K), the loss of water was observed to occur at higher temperatures for Pt3 (TGA). The total water weight loss in sample Pt2 was also slightly higher than that observed for Pt3. A higher H_2O/alkoxide ratio was used during the preparation of Pt3, so the remaining water was presumably removed during the drying step. The presence of solvents do not appear to have a major influence, as similar intensities in both samples were detected in the infrared spectra (Fig. 1).

With regard to the FTIR spectra, some interesting facts are observed in the samples dried at 393 K (Fig. 1). As described above, the band at $1080\,cm^{-1}$ is related to the bending of O–H bonds present in hydroxyl groups adjacent to the Al atoms and of O–H bonds corresponding to molecular water contained in the samples. This band appears to be shifted towards lower wavenumbers (higher

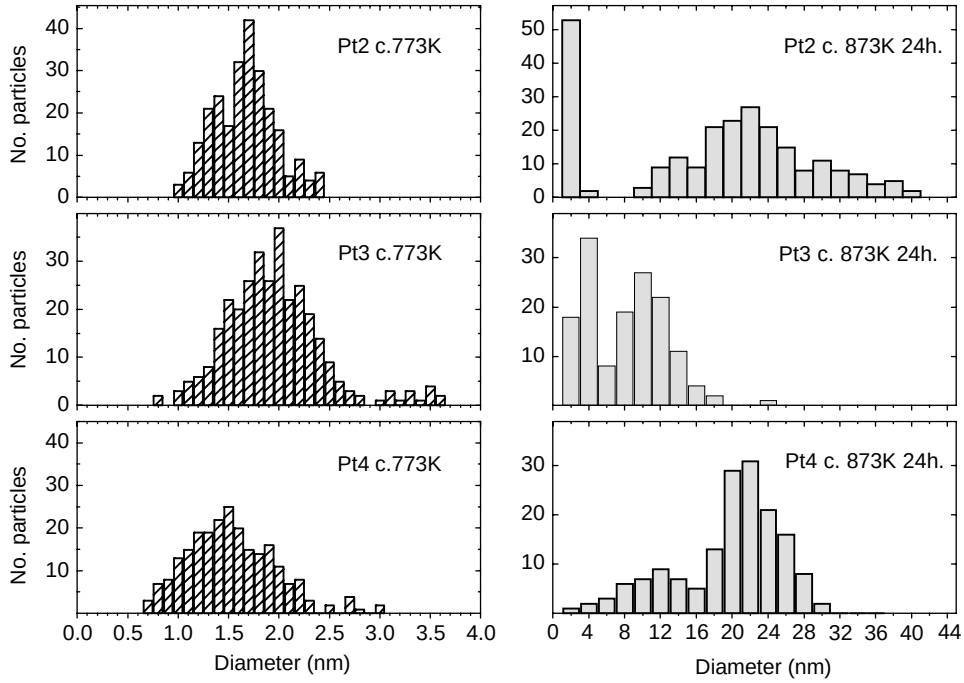

FIG. 8. Platinum particle size distribution following calcination at 773 K for 2 h and 873 K for 24 h.

bond energies) in the case of sample Pt3. Consequently, Pt3 exhibits more resistance to the bending (distortion) mode of O–H bonds. This can be related to a higher extent of interaction or, more probably, to a stronger interaction of H atoms with neighboring (oxygen) atoms (hydrogen bonds). Moreover, though hard to see, the shoulder at $3200\,m^{-1}$ appears with increased both intensity and width in Pt3. This effect is attributed to the O–H stretching vibration and may be related to the presence of O–H bonds with larger interatomic distances (22). On this basis, the shoulder at $3200\,cm^{-1}$ may be due to the presence of these O–H bonds. These bond distances may be larger than those observed at $3400\,cm^{-1}$. These larger distances may be the result of weak interactions with adjacent atoms (hydrogen bonds). However, other authors reported (in partially deuterated boehmite samples) that these two different distances are in fact coupled stretching modes of adjacent OH groups which have the same bond length (33). In any case, the shift of the band at $1080\,cm^{-1}$ remains significant, and gives evidence of a stronger interaction, or a higher extent of interaction, of coupled OH groups in sample Pt3.

For the samples calcined at 773 K (Fig. 5) no significant differences were detected between Pt2 and Pt3 in the range where Al–O vibration bands appear. The shoulder at $3200\,cm^{-1}$ showed a similar behavior to the dried sample, with a higher relative intensity (in comparison to the band at $3400\,cm^{-1}$) in Pt3 than Pt2.

As previously reported (11), the water/alkoxide ratio influences the structural properties of these sol–gel samples. Bradley *et al.* (34) reported that the initial oligomerization of the alkoxide determines the properties of the condensate (gel). Because of this, a simpler, more compressed structure (trimer) was proposed for the aluminum alkoxide used in this work (ATB) (35). A smaller steric effect allowing deeper hydrolysis than in larger oligomerized structures, in which hydrolysis can affect mainly the external departing groups, was proposed. Anyway, the steric crowding caused by the alkoxide ligand leads to a more difficult hydrolysis of the ATB molecule, which consequently limits the condensation step (36). Because of this, a higher water/alkoxide ratio would result in a greater extent of hydrolysis and condensation reactions, generating a more condensed product (36) and/or a material (gel) with higher pore surface tortuosity and/or roughness. In fact, Pt3 showed a slightly lower BET surface area than Pt2 following calcination at 773 K, even though both materials had a similar platinum content. The idea of a higher condensation or a larger pore tortuosity/roughness agree with a shift in the $1080\,cm^{-1}$ IR band for Pt3 (dried). It may also be related to the inhibition in the rate of OH removal from the pseudoboehmite structure of this sample in the TG-DTG experiments. The H_2O/ATB ratio of 9 not only resulted in a more condensed or winding structure, but also in a different and better-defined pore size distribution. This may affect the properties of the active metal contained within the alumina matrix. For this reason, the platinum particles showed a lower degree of sintering in Pt3 following aging. It has been previously reported (37) that when the metal crystallite size is of the order of magnitude of the pore diameter, surface diffusion of the crystallites on the support surface is decreased. Under these conditions, agglomeration of the Pt particles is reduced. This may be the case for sample Pt3, which exhibited a better, well-defined, and unimodal pore size distribution. It is also of interest to note that sintering stopped when the particle size was approximately equal to the pore diameter. The idea of a higher pore surface winding and roughness in Pt3 also agrees with the limit at which sintering stops.

Sample Pt3 also retained the highest BET surface area of the samples in which the metal precursor was H_2PtCl_6 following thermal treatment. Soled (38) claimed that transitional aluminas with BET surface areas in excess of $200\,m^2/g$ probably were due to a large extent of amorphous component. This conclusion was based on calculations which took into consideration the microcrystalline nature of γ-Al_2O_3. In general, surface areas in the neighborhood of $200\,m^2/g$ should be expected for γ-Al_2O_3. The lower initial weight loss TG–DTG in Pt3 might be related in some way to the lower BET surface area loss of this sample following aging at 873 K. The total weight loss in Pt3 during TG–DTG was also slightly lower (18.9%) than the other samples. Therefore, Pt3 catalyst can be stabilized at 873 K with more amorphous content than the others, and so it can exhibit a higher BET surface area.

CONCLUSIONS

The use of hexachloroplatinic acid (H_2PtCl_6) as the metal precursor resulted in materials with better catalytic properties (metallic dispersion) than those in which platinum acetylacetonate ($Pt(AcAc)_2$) was used. The sample prepared using a water/alkoxide ratio of 9 showed a higher thermal stability then catalysts prepared with H_2O/ATB = 3. It exhibited a lower relative loss in BET surface area and also a different (unimodal) and more uniform pore size distribution. This catalyst showed a more condensed or tortuous/rough pore structure following drying (as shown by FTIR). This enabled the retention of a more amorphous alumina structure following calcination and aging and consequently, a higher surface area than the other samples. This sample also showed a higher stability to Pt sintering following thermal treatment at 873 K.

ACKNOWLEDGMENTS

E. Romero-Pascual and A. Monzón thank DGESIC (Spanish Gov.) (project PB97-1020) for financial support. R. D. Gonzalez wishes to thank

the Basic Energy Sciences Division of the US Department of Energy for financial support. E. Romero-Pascual also gratefully thanks DGESIC for the grant which included a 3-month stay in the Department of Chemical Engineering of Tulane University, in New Orleans, USA.

REFERENCES

1. P. Degobert, "Automobiles and Pollution." Society of Automotive Engineers, Warrendale, PA, USA, 1995.
2. R. M. Heck and R. J. Farrauto, "Catalytic Air Pollution Control: Comercial Technology." Van Nostrand Reinhold, New York, 1995.
3. K. C. Taylor, *in* "Catalysis-Science and Technology" (J. R. Anderson and M. Boudart, Eds.), Chap. 2. Springer-Verlag, Berlin, 1984.
4. H. C. Yao and Y. F. Yu Yao, *J. Catal.* **86,** 254 (1984).
5. A. Trovarelli, C. de Leitenburg, and G. Dolcetti,, *Chemtech* **27,** 32 (1997).
6. S. Rossignol, F. Gerard, and D. Duprez, *J. Mater. Chem.* **9,** 1615 (1999).
7. M. F. L. Johnson, *J. Catal.* **123,** 245 (1990).
8. R. D. Gonzalez, T. Lopez, and R. Gomez, *Catal. Today* **35,** 293 (1997).
9. J. B. Miller and E. I. Ko, *Catal. Today* **35,** 269 (1997).
10. M. C. Couvillion, US Patent 4493906, 1985.
11. K. Balakrishnan and R. D. Gonzalez, *J. Catal.* **144,** 395 (1993).
12. M. F. L. Johnson and C. D. Keith, *J. Phys. Chem.* **67,** 200 (1963).
13. A. Bellare, D. B. Dadyburjor, and M. J. Kelley, *J. Catal.* **117,** 78 (1989).
14. E. Ruckenstein and M. L. Malhotra, *J. Catal.* **41,** 303 (1976).
15. F. H. Huang and C. Y. Li, *Scr. Metall.* **7,** 1239 (1973).
16. P. Wynblatt and N. A. Gjostein, *Scr. Metall.* **7,** 969 (1973).
17. L. Spenadel and M. Boudart, *J. Phys. Chem.* **64,** 204 (1960).
18. V. Alevra, D. Ciomirtan, and M. Ionesco, *Rev. Roum. Chim.* **17,** 1163 (1972).
19. B. C. Lippens and J. J. Steggerda, *in* "Physical and Chemical Aspects of Adsorbents and Catalysts" (B. G. Linsen, Ed.), p. 171. Academic Press, New York, 1970.
20. G. A. Dorsey Jr., *Anal. Chem.* **40,** 971 (1968).
21. M. C. Stegmann, D. Vivien, and C. Mazieres, *Spectrochim. Acta* **29A,** 1653 (1973).
22. J. Rouquerol, J. Fraissard, M.-V. Mathieu, J. Elston, and B. Imelik, *Bull. Soc. Chim. Fr.* 4233 (1970).
23. F. J. Shipko and R. M. Haag, KAPL Rept. 1740, General Electric Co., 1957.
24. B. C. Lippens and J. H. deBoer, *Acta Crystallogr.* **17,** 1312 (1964).
25. V. Alevra, D. Ciomirtan, and M. Ionescu, *Rev. Roum. Chem.* **17,** 1379 (1972).
26. L. L. Murrel, N. C. Dispenziere Jr., and K. S. Kim, *ACS Symp. Ser.* **437,** 97 (1990).
27. P. Reyes, M. Oportus, and B. Moraweck, *Catal. Lett.* **37,** 193 (1996).
28. M. Baltes, O. Collart, P. Van Der Voort, and E. F. Vansant, *Langmuir* **15**(18), 5841 (1999).
29. R. J. P. Lyon, "Evaluation of Infrared Spectrophotometry for compositional Analysis of Lunar and Planetary Soils." Stanford Research Institute Final Report under Contract NASr-49(04), published by N.A.S.A. as Technical Note D-1871, 1963.
30. S. Hafner, *Z. Kristallogr.* **115,** 331 (1963).
31. G. R. Wilson and W. K. Hall, *J. Catal.* **17,** 190 (1970).
32. F. M. Dautzenberg and H. B. M. Wolters, *J. Catal.* **51,** 26 (1978).
33. J. J. Fripiat, H. Bosmans, and P. G. Rouxhet, *J. Phys. Chem.* **71,** 1097 (1967).
34. D. C. Bradley, R. Gaze, and W. Wardlaw, *J. Chem. Soc.* 469 (1957).
35. O. Kriz, B. Casensky, A. Lycka, J. Fusek, and S. Hermanek, *J. Magn. Reson.* **60,** 375 (1984).
36. C. J. Brinker and G. W. Scherer, "Sol–Gel Science: The Physics and Chemistry of Sol–Gel Processing." Academic Press, New York, 1990.
37. E. Ruckenstein and B. Pulvermacher, *J. Catal.* **37,** 416 (1975).
38. S. Soled, *J. Catal.* **81,** 252 (1983).